JJMIE

Volume 16, Number 4, September. 2022
ISSN 1995-6665
Pages 543 – 556

Jordan Journal of Mechanical and Industrial Engineering

Impact of Discrete Multi-arc Rib Roughness on the Effective Efficiency of a Solar Air Heater

Arwa M. Kadhim, Mena S. Mohammed, Ammar A. Farhan*

Department of Energy Engineering, University of Baghdad, 10071, Baghdad, Iraq

Received 29 Mar 2022 *Accepted 14 Jun 2022*

Abstract

Artificial roughness on the absorber plate of a Solar Air Heater (SAH) is a popular technique for increasing its effective efficiency. The study investigated the effect of geometrical parameters of discrete multi-arc ribs (DMAR) installed below the SAH absorber plate on the effective efficiency. The effects of major roughness factors, such as number of gaps (N_g = 1-4), rib pitch (p/e = 4-16), rib height (e/D = 0.018-0.045), gab width (w_g/e = 0.5-2), angle of attack (α = 30°-75°), and Reynolds number (Re= 2000-20000) on the performance of a SAH are studied. The performance of the SAH is evaluated using a top-down iterative technique. The results show that as Re rises, SAH-effective DMAR's efficiency first ascends to a specified value of Re to attain the maximum values then falls. The useful energy gained via SAH-DMAR is higher by an average of 12% when compared to smooth SAH. According to the findings, the effective efficiency of SAH-DMAR is 9.4% higher than that of smooth SAH. The maximum thermal efficiency of SAH-DMAR and smooth SAH is 81.1 % and 74.7 %, respectively.

Keywords: SAH, effective efficiency, DMAR, rib roughness.

Nomenclature

A_p	aperture area of the SAH (m^2)
b	half-height of the v-channel (m)
cp_a	specific heat of the air (J/kg K)
D	hydraulic diameter
e/D	rib height
f	friction factor
h_1	coefficient of convective heat transfer between the absorber plate and air (W/m^2 K)
h_2	coefficient of convective heat transfer between the bottom plate and air (W/m^2 K)
h_r	coefficient of radiative heat transfer between absorbing and bottom plates (W/m^2 K)
h_w	coefficient heat transfer of wind (W/m^{2}K)
I	insolation (W/m^2)
k_a	thermal conductivity of air (W/m K)
k_i	thermal conductivity of the glass wool (W/m K)
L_c	Length of SAH (m)
$\dot{m}_a$	air mass flow rate (kg/s)
N_g	gap numbers
Nu	Nusselt number
p/e	rib pitch
P_m	mechanical power consumed by the fan (W)
Q_u	useful energy (W)
Re	Reynolds number
T_a	air temperature (K)
T_{ai}	inlet air temperature (K)
T_{am}	ambient temperature (K)
T_{ao}	outlet air temperature (K)
T_{mb}	bottom plate temperature (K)
T_{mp}	absorber plate temperature (K)
t_i	bottom insulation thickness (m)
U_b	coefficient of bottom heat loss (W/m^2 K)
U_t	coefficient of top heat loss (W/m^2 K)
V_{in}	inlet air velocity (m/s)
V_w	wind speed (m/s)
W_c	Width of SAH (m)

Greek letters

α_p	absorber plate absorptance
β	collector inclined angle (°)
σ	Stefan–Boltzmann constant (W/m^2 K^4)
ρ_a	air density (kg/m^3)
μ_a	air viscosity (Pa s)
η_t	Thermal efficiency (%)
ε_p	absorber plate emittance
ε_b	back plate emittance
τ_c	cover transmittance
ε_c	cover emittance
η_{eff}	effective efficiency (%)
ΔP	pressure drop (Pa)

1. Introduction

Significant energy demand due to population increase has resulted in an unsustainable reliance on rapidly depleting fossil fuel reserves. Because of increased consumption, prices are expected to soar, maybe above inflation. Additionally, because of the environmental threat posed by this, the world society has been driven to adopt renewable energy as a means of attaining sustainable growth[1,2]. Solar energy is a sustainable source of energy that produces no pollution. It is employed in a wide variety of residential and industrial applications[3–5].

Solar air heaters (SAHs) are a type of heat exchanger that captures solar energy and transmit it to the air moving through them[6]. SAH is simple to produce and affordable

* Corresponding author e-mail: ammarali@uobaghdad.edu.iq.

to manufacture. It has a few drawbacks; one of which is that the poor coefficient of heat transfer between the heated absorber plate and the working fluid (air) results in higher heat loss and decreased efficiency. This is because the laminar sub-layer imposes a high thermal resistance on the heat transfer process [7,8]. Researchers have used both passive and active heat transfer augmentation approaches to break through this sub-layer, with passive heat transfer enhancement techniques being the most commonly investigated [9,10]. In this scenario, ribs were utilized to restrict the flow, which resulted in the separation and subsequent reattachment of the boundary layer, leading to higher turbulence.

Numerous rib configurations have been investigated numerically and experimentally to increase the rate of convective heat transfer. Initially, continuous ribs perpendicular to the main flow stream were utilized to boost the convective heat transfer rate of the turbulent flow duct [11–13]. However, any significant improvement in overall performance was offset by the larger pressure drop associated with the addition of ribs. Later, discrete ribs were used to reduce the higher pressure drop caused by the blocking effect of the ribs [10,14,15]. Saini and Saini [16] experimentally discovered that arc-shaped ribs in rectangular ducts increased the Nusselt number (Nu) by an order of 3.6 and the friction factor by 1.75 times when compared to a smooth channel. Ghritlahre et al.[17] implemented an experimental investigation on apex up and apex down ribs which give enhancement in heat transfer as compared to smooth duct SAH. Multiple arc-shaped ribs were employed by Singh et al. [18] on a heated plate with a rectangular channel. In comparison to a smooth surface, the greatest increase in Nu and friction factor was found to be 5.07 and 3.71 times.

Experiments were conducted by Pandey and Bajpai [19] to examine the thermal performance of a SAH with multi-arc-shaped ribs with gap roughness on the absorber plate. The result shows that, as the Reynolds number (Re) increases from 2100 to 21000, the thermal performance of the roughened collector is found to increase from 0.37 to 0.83, compared to 0.21 to 0.55 for the smooth SAH. Kumar et al. [12] investigated heat transfer and friction in the flow of air via rectangular ducts with S-shaped ribs on the absorber plate. The result indicates that the Nu and friction factors rise by a maximum of 4.64 and 2.71 times, respectively. Additionally, correlations for the Nu and friction factor were developed. Agrawal et al. [20] conducted experiments to determine the impact of geometrical parameters on the heat transfer coefficient and thermal efficiency of artificial roughness with a discrete double arc reverse shape. It was reported that the largest improvements in heat transfer coefficient and thermal efficiency over a smooth duct are 2.88 and 1.29, respectively. Multiple-arcrib roughness patterns with gap-shaped roughness were studied experimentally by Kumar et al. [21]. The proposed roughed solar air heater has a Nu and friction factor that are 5.76 and 6.05 times higher than the smooth SAH.

A comprehensive study of the literature carried out by Nidhul et al. [3] reveals that the arc-shaped rib pattern is superior to other rib patterns, such as a wedge, transverse, and rib-groove combination roughness. Azad et al. [22] conducted an experimental investigation on a solar air heater with a new discrete symmetrical arc rib design. The Nu and friction factor were found to be 2.26 and 3.87 times greater than those of a smooth duct, respectively. Bhuvad et al. [14] investigated the thermal-hydraulic performance of a solar air heater equipped with a new apex-up discrete arc rib roughness on the backside of the absorbing plate. At a 30° angle of attack, the maximum enhancement in thermal-hydraulic performance is 2.01. V-groove absorbing plate have also been employed to increase the surface area available for heat transfer in several studies. As a result of the increased surface area, the rate of heat transfer becomes more efficient. A V-groove absorbing plate is more efficient in absorbing heat. As the absorption rate increases, the heat transfer area of the corrugated surfaces practically doubles, increasing the temperature of the absorber plate [23].

According to the literature, artificial ribs on the absorbing surface are an effective method to enhance SAH heat efficiency. As a result, pressure drop throughout the system has increased significantly, resulting in higher power usage. In the present work, the effects of discrete multi-arc rib roughness on SAH are studied for a variety of Re values ranging from 2000 to 20000. The effect of geometrical parameters of the DMAR like N_g, p/e, w_g/e, e/D, and α on the thermal performance of the V-groove SAH is numerically investigated and validated in actual weather conditions. In addition, the effective efficiency of the SAH roughened by DMAR is estimated using a top-down iterative technique. To the best of the author's knowledge, no research study has documented the use of discrete multi-arc rib roughnesswith V-groove SAH.Thereby, the work's originality is evident in its contribution to this field of study.

2. Analytical methodology

2.1. Mathematical model

It is expected that SAH with artificial roughness will perform better than smooth surface SAH. Because of turbulence in the viscouslayer, heat transport is significantly improved. Additionally, a SAH with a triangle duct provides superior thermal performance than a SAH with a rectangular duct [13]. Fig. 1 shows a V-groove SAH having discrete multi-arc rib roughness on the absorbing plate. A 60-degree corrugation angle V-groove SAH has a 4 mm glass cover, a 1 mm absorber and backplates, and a 50 mm backside insulation. The absorber and bottom plates combine to produce a triangle-shaped duct that allows air to move through the SAH. Two identical V-groove SAHs are compared: one with discrete multi-arc rib roughness and the other without. Following are the assumptions that were made to derive the energy balance equation for each element of the V-groove SAH without altering the fundamental physical situation [24].

1. The steady-state assumption is used in the modeling of the V-groove SAH.
2. In a CV-groove SAH, one-dimensional heat transfer takes place between the various components of the system.
3. The side heat losses of the V-groove SAH are neglected, and there is no air leakage from the SAH.

The thermal behavior of the SAH with a roughened heated surface is the same as that of the smooth SAH. When insolation strikes the absorber plate, it is absorbed and then transferred to the working fluid. As a result, the same approach that is used to calculate temperatures and heat losses for smooth SAH may also be applied to roughened SAH. Fig. 2 depicts an energy flow between SAH components. Following the energy flow schematic, the energy equations for the absorbing plate, air, and bottom plate per unit area are expressed as follows:

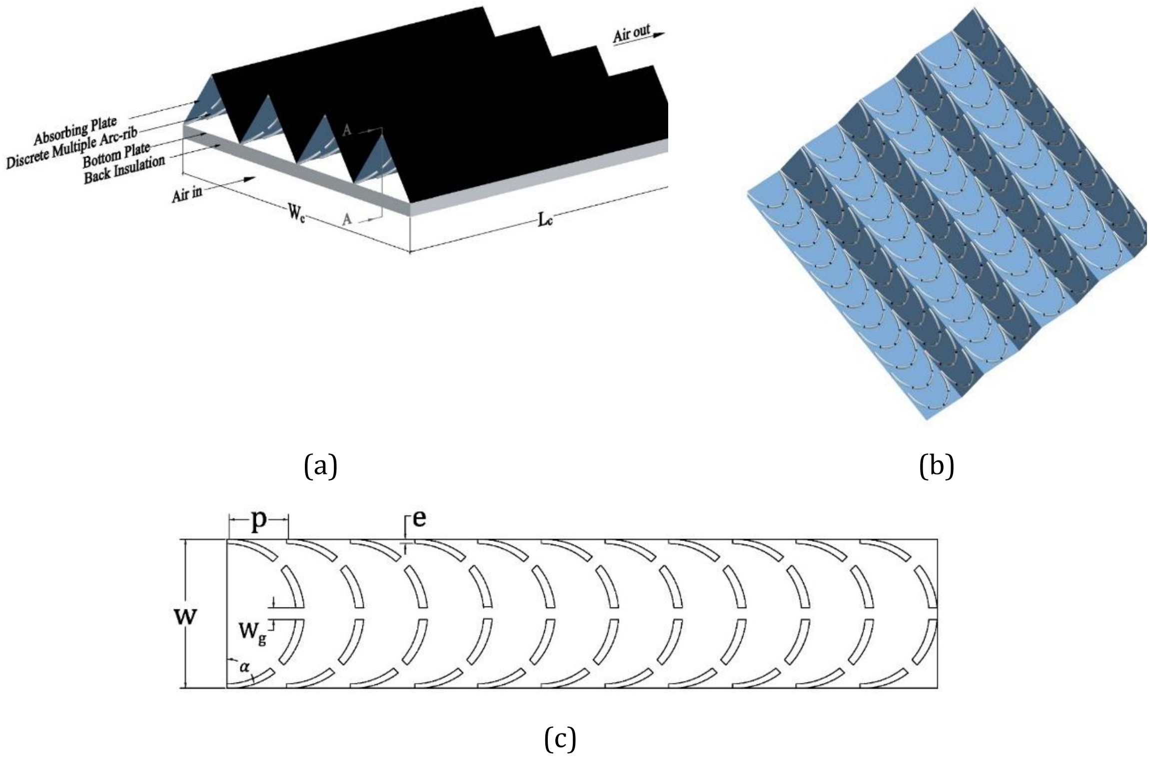

Figure 1. Schematic diagram of (a) SAH elements, (b) discrete multi-arc ribs on the backside of the absorbing plate, and (c) cross-sectional view of A-A

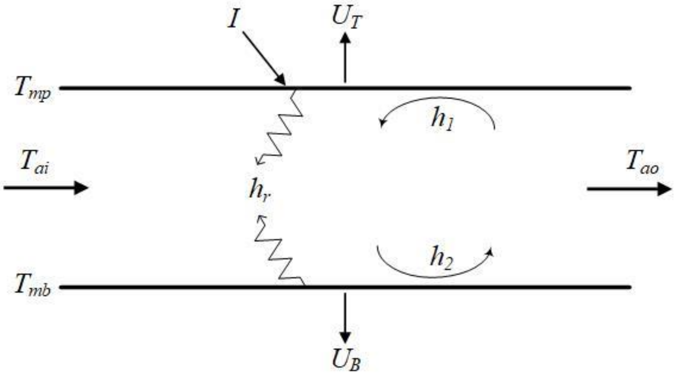

Figure 2. Schematic representation of the flow of energy between SAH components.

$$\tau_c\, \alpha_p I - U_T\left(T_{mp} - T_{am}\right) - h_r\left(T_{mp} - T_{mb}\right) - h_1\left(T_{mp} - T_a\right) = 0 \tag{1}$$

$$\frac{2\dot{m}_a c p_a}{A_p}\left(T_a - T_{ai}\right) - h_1\left(T_{mp} - T_a\right) - h_2\left(T_{mb} - T_a\right) = 0 \tag{2}$$

$$h_r\left(T_{mp} - T_{mb}\right) - h_2\left(T_{mb} - T_a\right) - U_B\left(T_{mb} - T_{am}\right) = 0 \tag{3}$$

2.2. Performance parameters of a SAH

The simplest approach to comparing the performance of a SAH is to examine its thermal efficiency. However, a SAH duct with artificial roughness led to better heat transfer, which also led to a boost in pumping power. Effective performance is based on how much energy is gained by air and how much more power is needed to pump air. Both the thermal and effective performance of the SAH should be considered when trying to find the best roughness parameters.

SAH thermal efficiency is the ratio of useful thermal energy gained by the air to the rate of solar energy that hits the heater's aperture, and is given as:

$$\eta_t = \frac{Q_u}{IA_p} = \frac{\dot{m}_a cp_a (T_{ao} - T_{ai})}{IA_p} \tag{4}$$

According to Cortes and Piacentini[25] hypothesis, SAH's net usable gain should be defined in terms of both thermal gain and the blower power consumption. As a result of the increased convective heat transfer coefficient, artificial roughness on the absorber plate improves thermal efficiency. However, this leads to a rise in pressure drop, which means that more mechanical power is needed to move air through the collector's duct. Typically, mechanical power (P_m) is provided by a blower powered by an electrical motor. It is, therefore, impossible to establish how much useful energy is gained by subtracting the motor's electrical energy consumption from the collector's thermal energy gain. The collector's energy losses must be considered when calculating the collector's net heat gain. The equivalent thermal energy (ETE) necessary to overcome friction is denoted by the following formula:

$$ETE = \frac{P_m}{\eta_{net}} \tag{5}$$

Where η_{net} is the net efficiency of converting thermal energy to mechanical energy conversion and is calculated as follows:

$$\eta_{net} = \eta_b \eta_m \eta_{tr} \eta_{thp} \tag{6}$$

Cortes and Piacentini[25] stated that the normal value of η_{net}, based on the common efficiency of several processes, such as blower efficiency η_b = 0.65, electric motor efficiency η_m = 0.88,the efficiency of electrical transmission from the power plant η_{tr} = 0.925, andthe thermal conversion efficiency of the power plant η_{thp} = 0.344, is 0.18.

The effective efficiency (η_{eff}) is defined as the ratio of net useful thermal energy gained by the air to the rate of insolation on the aperture of the collector, and is expressed as:

$$\eta_{eff} = \frac{Q_u - ETE}{IA_p} \tag{7}$$

2.3. Procedure for prediction of performance

Different system and operating parameters were used to determine the thermal and effective efficiencies of a SAH. Performance evaluation of a SAH is quantitatively carried out by a top-down iterative technique using MATLAB. The following process details the steps involved in calculating thermal and effective efficiency for a given set of roughness and operational parameter values:

Step 1. Selected values of roughness and operating parameters have been chosen such as p/e, Ng, e/D, α, w_g/e, Re, and I, as shown in Table 1.

Table 1. Design parameter data for the prediction model.

Parameter	Value
Length of SAH (L_c)	1 m
Width of SAH(W_c)	0.4 m
Rib pitch (p/e)	4-16
Rib height (e/D)	0.018-0.045
Rib width (W_p/w)	8
Gap numbers (N_g)	1-4
Gap width (w_g/e)	0.5-2
Angle of attack (α)	30°-75°
Bottom insulation thickness (t_i)	0.05 m
Thermal conductivity of glass wool (k_i)	0.034 W/m.°C
Absorbing plate emittance (ε_p)	0.95
Back plate emittance (ε_b)	0.95
Absorber plate absorptance (α_p)	0.96
Cover emittance (ε_c)	0.9
Cover transmittance (τ_c)	0.88
Reynolds number (Re)	2000 – 20,000
Insolation (I)	1000 W
Ambient temperature (T_{am})	25°C
Inlet air temperature (T_{ai})	25°C
Wind velocity (V_w)	2.5 m/s

Step 2. To begin the calculation, arbitrary values of T_{pm} (mean absorber plate temperature),T_{ao} (outlet air temperature), and T_{mb} (mean bottom plate temperature) are used as follows[26]:

$$T_{mp} = T_{am} + 20 \tag{8a}$$

$$T_{ao} = T_{am} + 10 \tag{8b}$$

$$T_{mb} = T_{am} + 10 \tag{8c}$$

Inlet air temperature is equal to ambient temperature, and mean air temperature (T_m) is used to evaluate the thermo-physical properties of air [27].

$$\rho_a = 1.1774 - 0.000066(T - 27) \tag{9a}$$

$$k_a = 0.02624 + 0.0000758(T - 27) \tag{9b}$$

$$\mu_a = [1.983 + 0.00184(T - 27)]10^{-5} \tag{9c}$$

$$cp_a = 1.0057 + 0.000066(T - 27) \tag{9d}$$

Step 3. Heat transfer coefficientsare calculated as follows:

The top heat loss coefficient (U_T) is obtained by combining $T_{mp}$and $T_{am}$with the correlation reported by Duffie et al. [26]

$$U_T = \left[\frac{M}{\left(\frac{C}{T_{mp}}\right)\left(\frac{T_{mp}-T_{am}}{M+f_m}\right)^{0.33}} + \frac{1}{h_w}\right]^{-1} + \left[\frac{\sigma(T_{mp}^2+T_{am}^2)(T_{mp}+T_{am})}{\frac{1}{\epsilon_p+0.05M(1-\epsilon_p)}+\frac{2M+f_m-1}{\epsilon_c}-M}\right] \tag{10a}$$

where,M is the number of glass covers.

$$C = 204.429\,(\cos\beta)^{0.252} L^{-0.24} \tag{10b}$$

$$f_m = \left(\frac{9}{h_w} - \frac{30}{h_w^2}\right)\left(\frac{T_{am}}{316.9}\right)(1 + 0.091M) \tag{10c}$$

$$h_w = 5.3 + 3.7\,V_w \tag{10d}$$

The bottom heat loss coefficient (U_B) is calculated by combining the thermal conductivity (k_i) and the thickness (t_i) of the insulation[26].

$$U_B = \frac{k_i}{t_i} \quad (11)$$

The overall heat loss coefficient (U_L) is estimated as:

$$U_L = U_T + U_B \quad (12)$$

The thermal radiation coefficient (h_r) between the absorber and backplates can be estimated as:

$$h_r = \frac{\sigma(T_{mp}^2+T_{mb}^2)(T_{mp}+T_{mb})}{\frac{1}{\epsilon_p}+\frac{1}{\epsilon_b}-1} \quad (13)$$

Re for equilateral triangular duct is computed as

$$\mathrm{Re} = \frac{4\,\rho_a V_{in} b}{3\,\mu_a} \quad (14)$$

where b is the half-height of the triangular duct.

For Nusselt number (Nu) inside the triangle conduit of the smooth SAH, Hollands and Shewen [28] proposed the following relationship to compute the convective heat transfer coefficient (h_1) between absorbing plate and air.

$$\mathrm{Nu}_1 = \mathrm{Nu}_o + \gamma_o \frac{b}{L_c} n, \quad (15)$$

where n is the number of collectors connected in series, and Nu_o and γ_o are functions of Re. Hollands and Shewen [28] recommended the following relations for Nu_o and γ_o:

$$\mathrm{Nu}_o = 2.821 \text{ and } \gamma_o = 0.126\mathrm{Re} \text{ for } \mathrm{Re} < 2800, \quad (16a)$$

$$\mathrm{Nu}_o = 1.9 \times 10^{-6}\mathrm{Re} \text{ and } \gamma_o = 225 \text{ for } 2800 \le \mathrm{Re} \le 10^4, \quad (16b)$$

$$\mathrm{Nu}_o = 0.0302\mathrm{Re}^{0.74} \text{ and } \gamma_o = 0.242\mathrm{Re}^{0.74} \text{ for } 10^4 < \mathrm{Re} < 10^5. \quad (16c)$$

An empirical equation, which was correlated by Kumar et al. [21], is used to determine the Nu_r for a SAH roughened by discrete multi-arc ribs on the absorbing plate as formula 17:

The Dittus-Boelter equation for Nu_2 is used to calculate the convective heat transfer coefficient (h_2) between the bottom plate and air [26].

$$Nu_2 = 0.023\, Re^{0.8}\, Pr^{0.4} \quad (18)$$

According to Hedayatizadeh [29], the coefficient of convective heat transfer is computed as follows:

$$h = \frac{3\,Nu\,k_a}{4\,b} \quad (19)$$

Step 4. The energy balance Eqs. (1-3) are solved by a top-down iterative program to yield new values for T_{mp}, T_{ao}, and T_{mb}. Compare these numeric values to the old ones. The comparison is based on the error value, which is the difference between the previous and current values. The procedure is repeated until all SAH temperature values are equal to or less than 0.00001.

Step 5. The value of friction factor (f_r), for the selected set of roughness parameters, is determined by the correlation developed by Kumar[21]. Whilst, f_s for smooth plate is determined using Hedayatizadeh et al. [29]relations.

$$f_s = f_o + \phi \frac{b}{L_c} n \quad (21)$$

f_o and $\phi$are functions of the Re number, determined as:

$$f_o = 13.33\mathrm{Re}^{-1} \text{ and } \phi = 0.65 \quad \text{for } \mathrm{Re} < 2800 \quad (22a)$$

$$f_o = 3.2 \times 10^{-4}\mathrm{Re}^{0.34} \text{ and } \phi = 2.94\mathrm{Re}^{-0.19} \text{ for } 2800 \le \mathrm{Re} \le 10^4 \quad (22b)$$

$$f_o = 0.0733\mathrm{Re}^{-0.25} \text{ and } \phi = 0.51 \text{ for } 10^4 \le \mathrm{Re} \le 10^5 \quad (22c)$$

The pressure drop across the duct (ΔP) can be calculated as follows [10]:

$$\Delta P = \frac{3\rho_a L_c V_{in}^2 f}{2b} \quad (23)$$

The amount of P_m required by the blower to force air throughout the SAH can be expressed as [30]:

$$P_m = \frac{\dot{m}_a\,\Delta P}{\rho_a} \quad (24)$$

Finally, useful energy gain, thermal, and effective efficiencies are calculated by Eqs. 4 and 7, respectively.The flowchart of the top-down iterative program is shown in Fig. 3.

$$\mathrm{Nu_r} = 7\times10^{-5}\left(\begin{array}{c} \mathrm{Re}^{1.557}\left(\frac{\mathrm{w_g}}{\mathrm{e}}\right)^{0.028}\mathrm{N_g}^{0.153}\left(\frac{\mathrm{W_p}}{\mathrm{w}}\right)^{0.075}\left(\frac{\alpha}{60}\right)^{0.153}\left(\frac{\mathrm{p}}{\mathrm{e}}\right)^{0.385}\left(\frac{\mathrm{e}}{\mathrm{D}}\right)^{0.231} \\ \times\exp(-0.22\ln\left(\frac{\mathrm{w_g}}{\mathrm{e}}\right)^2)\exp(-0.75\ln(\mathrm{N_g})^2)\exp(0.274\left(\ln\left(\frac{\alpha}{60}\right)\right)^2) \\ \times\exp\left(-0.0001\left(ln\left(\frac{\mathrm{W_p}}{\mathrm{w}}\right)\right)^2\right)\exp(-0.075\left(\ln\left(\frac{\mathrm{p}}{\mathrm{e}}\right)\right)^2) \end{array}\right) \quad (17)$$

$$f_r = 0.335\left(\begin{array}{c} \mathrm{Re}^{-0.25}\left(\frac{\mathrm{w_g}}{\mathrm{e}}\right)^{0.029}\mathrm{N_g}^{0.069}\left(\frac{\mathrm{W_p}}{\mathrm{w}}\right)^{0.079}\left(\frac{\alpha}{60}\right)^{0.132}\left(\frac{\mathrm{p}}{\mathrm{e}}\right)^{0.331}\left(\frac{\mathrm{e}}{\mathrm{D}}\right)^{0.156} \\ \times\exp(-0.152\ln\left(\frac{\mathrm{w_g}}{\mathrm{e}}\right)^2)\exp(-0.02\ln(\mathrm{N_g})^2)\exp(0.148\left(\ln\left(\frac{\alpha}{60}\right)\right)^2) \\ \times\exp\left(-0.004\left(ln\left(\frac{\mathrm{W_p}}{\mathrm{w}}\right)\right)^2\right)\exp(-0.068\left(\ln\left(\frac{\mathrm{p}}{\mathrm{e}}\right)\right)^2) \end{array}\right) \quad (20)$$

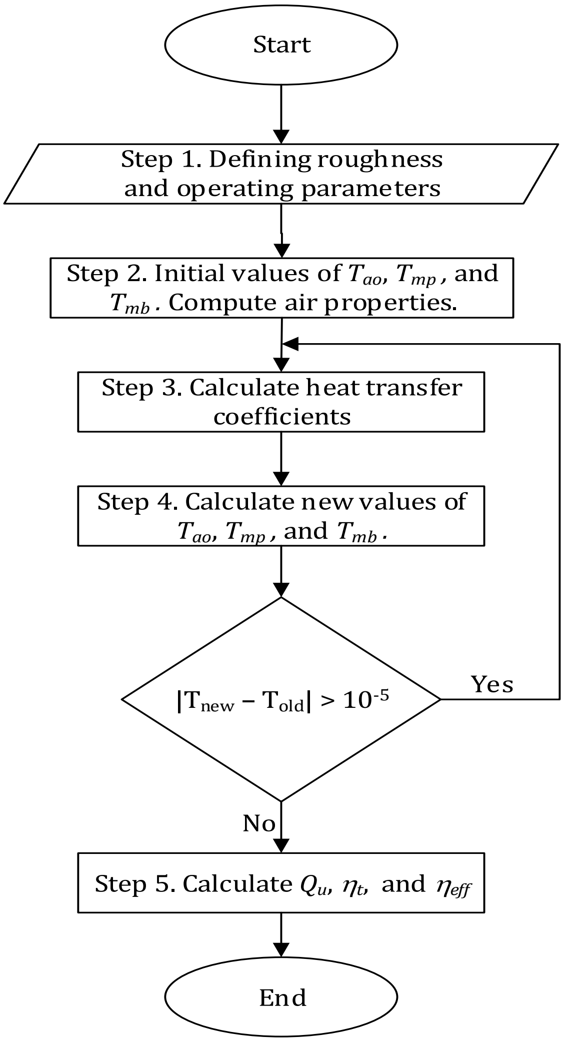

Figure 3. Flowchart for the computer program.

3. Results and discussion

The numerical solutions for different Re and roughness characteristics, such as rib height (e/D), number of gaps (N_g), gap width (w_g/e), ribpitch (p/e), and arc-angle (α) were used to calculate the T_p, Q_u, η_t, and η_{eff} of SAH roughened by DMAR, which were described further below. The results were compared to those obtained in the case of smooth ducts operating under the same conditions to investigate the improvement in T_{mp}, Q_u, η_t, and η_{eff} due to artificial roughness parameters.

Fig.4a depicts the impacts of the rib height(e/D) on the absorber plate temperature (T_p) vs the Re for the smooth SAH and SAH-DMAR at constant value of N_g = 2, w_g/e = 1.25, p/e = 10, and α = 45°. When the Re is increased, the absorber plate temperature declines dramatically at first, and then very minimally at high values of Re. The absorber plate temperature of the SAH-DMAR is lower than that of the smooth collector for a given Re. The temperature of the absorber plate drops when the diameter of the roughness element, which is represented by the dimensionless term e/D, is increased. For e/D = 0.045, the lowest absorber plate temperatures are 32.01 °C, compared to 42.77 °C for smooth SAH. This reduction in the temperature of the absorber plate is caused by the breakdown of a viscous sub-layer, which prevents heat transfer from the absorbing plate to the working fluid. As a result of the roughened absorbing plate, there has been an increment in the amount of useful energy (Q_u) gained by the air as shown in Fig. 4b. It can be seen that the enhancement in thermal energy gained by air is greatest at low Re and gradually diminishes until it becomes unchangeable at Re greater than 13000. When the diameter of the roughness element is increased, the thermal energy gain increases proportionally. The reason for this is that the low e/D is immersed in the viscous sublayer. In the case of e/D = 0.045, the highest thermal energy output value is obtained at 324.16 W, which is about 8.5% greater than the value obtained with smooth SAH.

For a wide variety of e/D, the influence on thermal efficiency (η_t) is shown in Fig. 5a. The thermal performance of roughened collector is higher than that of a smooth collector, as seen in the figure. This is owing to the fact that the heightening of DMAR helps in breaking down thermal resistance at the heating surface which promotes more heat transfer from the absorbing plate to the air. As a result, thermal efficiency is improved. When Re is raised from 2000 to 20000, the maximum thermal efficiency of a roughened collector increases from 49% to 81%, corresponding to an e/D value of 0.045. Thermal efficiency increases from 47.9% to 74.7% with Re for a smooth collector. SAH thermal performance is improved due to the DMAR arrangement over the absorber plate, which allows for recurrent breakage of viscous sub-layers. In contrast, the alteration in viscous sub-layers also encourages the production of small eddies near the roughness elements, which resulted in a greater pressure drop in the SAH. Thus, to select the best value of e/D, effective efficiency (η_{eff}) is plotted against Re as shown in Fig. 5b. Better effective efficiency is associated with increased e/D and/or a higher Re. As Re approaches 13000, efficiency begins to decline for all e/D levels. Further increases in Re (above 13000) may lead to extra frictional losses that are greater than the gain in heat transfer; consequently, a decrease in effective efficiency is observed. Effective efficiency for SAH-DMAR at e/D = 0.045 is 76.6 %, while the smooth SAH has an efficiency of 70.4%. These findings showed that the optimal effective efficiency is achieved at e/D = 0.045.

Fig. 6a depicts the effect of changing gap numbers (N_g) on absorbing plate temperature. Other roughness parameters are kept constant i.e.,e/D = 0.045, w_g/e = 1.25, p/e = 10, and α = 45°throughout the investigation. As N_g increases from 1 to 3, the temperature of the absorbing plate falls, until it reaches its minimum value of 31.9 °C at N = 3. However, as the value of N_g rises over 3, the temperature of the absorbing plate rises. This can occur as a result of the roughness-elements changing discharge points. The N_g serves as discharge points, allowing the secondary flow to depart through the DMAR. The number of discharge points in the DMAR grows as the value of N_g grows. However, the absorbing plate temperature only decreased up to N_g = 3 as can be shown. This could be owing to increased local turbulence strength caused by secondary flow discharged through gaps downstream of the DMAR. Also, it could be attributed to the transverse plane's highly intense swirl flow. When N_g> 3, the secondary flow may not be strong enough to cause additional turbulence at the rib downstream, resulting in higher absorbing plate temperatures. For varying values of Ng, Fig. 6b demonstrates the fluctuation of Q_u with Re while keeping the rest roughness parameters constant. It is clear that Q_u grows for a given number of gaps until it reaches 3, after which it decreases. It can be observed that the increase in thermal energy absorbed by air is largest at Re < 10000, as opposed to Re > 10000. The gaps break down the secondary flow along the ribs, allowing the secondary flow fluid to mix with the main flow. Consequently, Q_u is increased. The maximum value of Q_u is 324.2 W is obtained at Re = 20000 and N_g = 3.

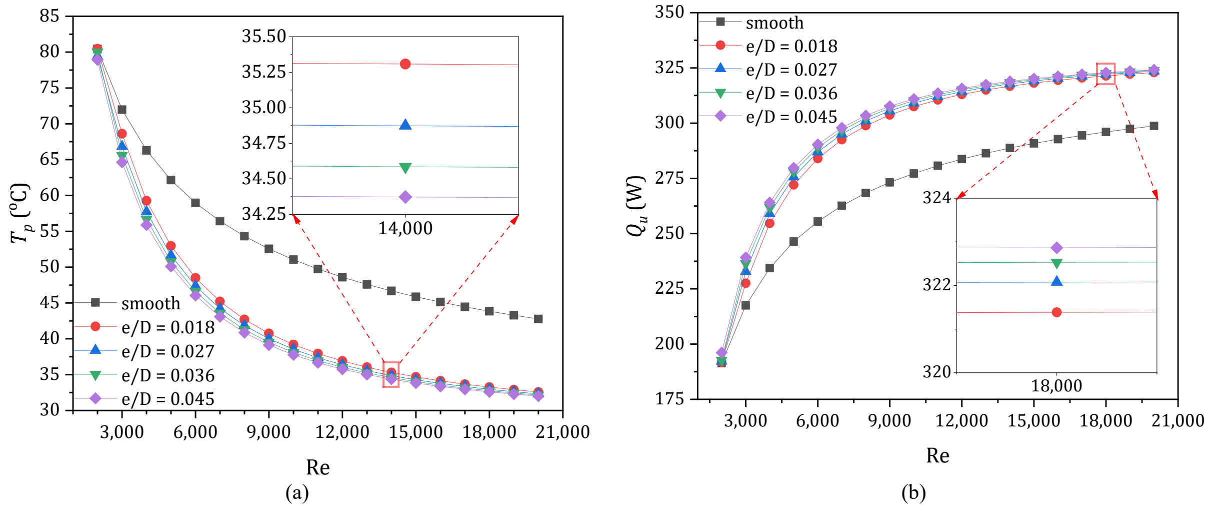

Figure 4. The effect of the e/D on (a) absorber plate temperature, and (b) useful energy gain.

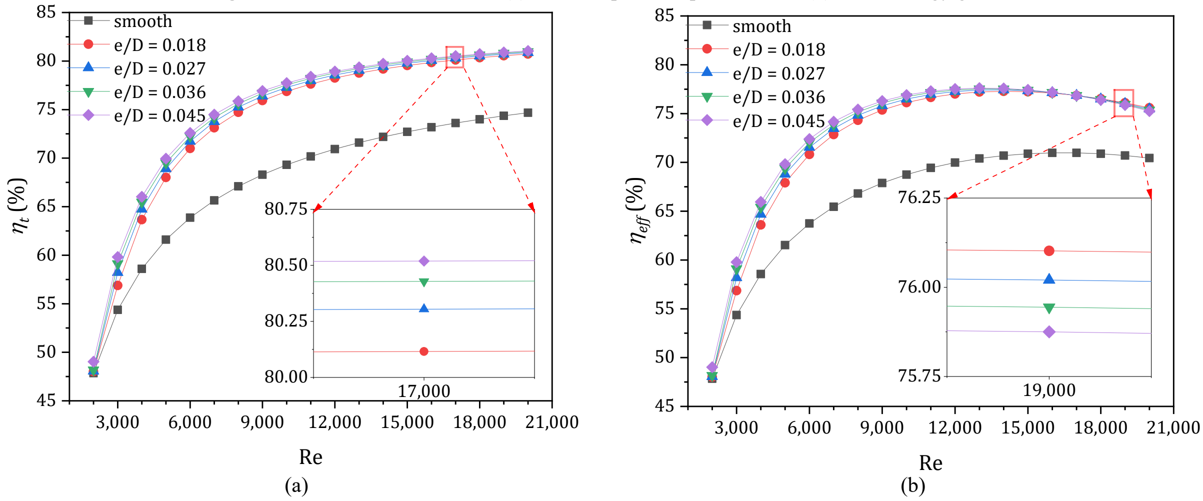

Figure 5. The influence of *e/D* on (a)thermal efficiency, and (b)effective efficiency.

The influence of N_g on thermal efficiency is demonstrated in Fig. 7a. As shown in the figure, the thermal performance of a roughened collector is better than that of a smooth collector. This is because N_g assists in mixing secondary flow along the ribs with the main flow through the duct, allowing for more heat transfer from the absorber plate to the air. Therefore, thermal efficiency enhances. Furthermore, with all Re studied, thermal efficiency improves as N_g increases until N_g = 3, and the opposite trend is observed at higher N_g values. At Re = 20000 and N_g =3, it can be seen that the thermal efficiency of SAH-DMAR is 7.9% higher than that of smooth SAH. Fig. 7b shows the difference in effective efficiency between a SAH with and without DMAR throughout a range of Re. Effective efficiency is significantly increased for all N_g values when compared to smooth SAH until Re = 13000 when it begins to decline because of the larger pressure drop when compared to lower thermal enhancement. The best effective efficiency for SAH-DMAR is 77.6%, compared to 70.4 % for a smooth SAH at Re of 13000. Maximum effective efficiency is found at Ng of 3 based on the above findings.

Fig. 8a depicts the effect of gap width (w_g/e) on T_p for constant values of e/D, N_g, p/e, and α, i.e., 0.045, 3, 10, and 45°. It can be noted that the T_p is lowest when w_g/e = 1, and largest when w_g/e = 0.5. The amount of flow rate that occurs at the rib downstream changes dramatically when the width of the given gaps in the DMAR is changed. It is necessary for the flow leaving via the gaps to have a higher velocity at the rib downstream for better heat augmentation. Because the gap width (w_g) for w_g/e< 1 is relatively small, the secondary flow flowing along the rib-element is unable to find a smooth path through it, resulting in a large T_p. When w_g/e > 1, the w_g becomes large enough to allow a smooth secondary flow outflow from the gap, but the flow is delayed, and the T_p rises. Because the absorber plate temperature is lower, more heat gain is absorbed by the air as shown in Fig. 8b. The smooth SAH pattern has the lowest heat gain when compared to the roughened SAH pattern, which increases as Re rises, especially at low flow rates. The maximal heat gain for a SAH-DMAR is 324.2 W, compared to 298.7 W for a smooth duct, as shown in Fig. 8b.

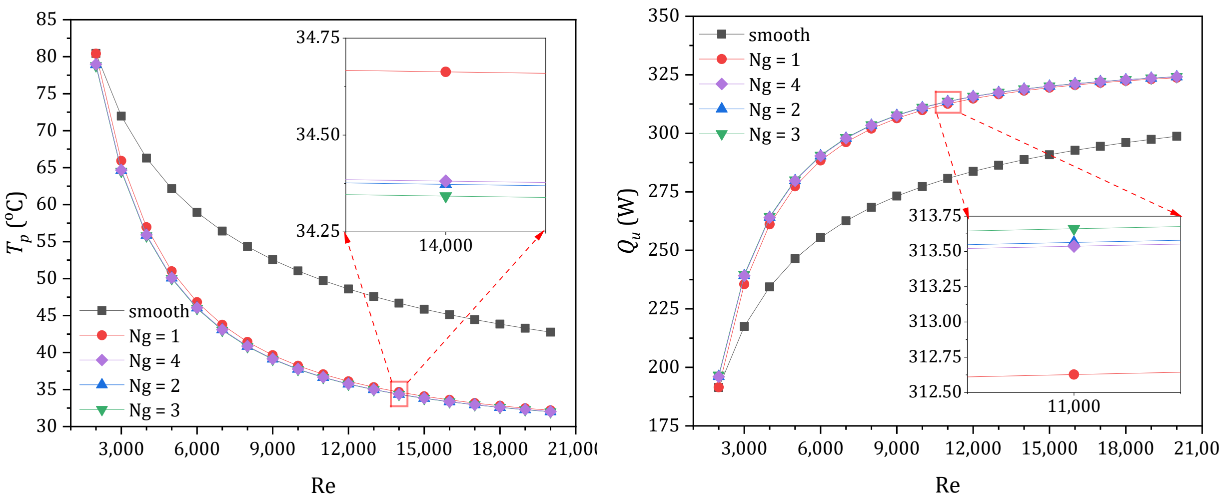

(a) (b)

Figure 6. The effect of the N_g on (a) absorber plate temperature, and (b) useful energy gain.

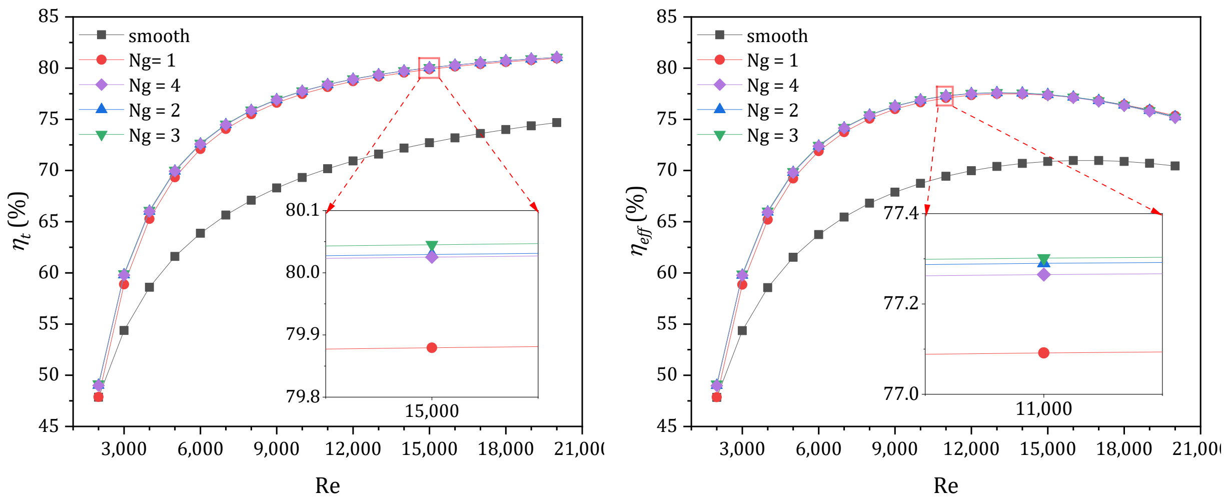

(a) (b)

Figure 7. The impact of N_g on (a)thermal efficiency, and (b)effective efficiency.

The influence of the w_g/e on the SAH's thermal efficiency for a wide range of Re is shown in Fig. 9a. With rising Re, the thermal efficiency rises dramatically as a result of the increased heat gain. Furthermore, as Re approaches 3000, the effect of DMAR on thermal efficiency becomes more substantial in comparison to the smooth duct. Furthermore, until w_g/e = 1, thermal efficiency improves as w_g/e increases, while the opposite tendency is observed for higher w_g/e values. In Fig. 9b, effective efficiency is plotted against Re for all w_g/e ratio values. Greater effective efficiency is associated with higher Re. This pattern continues until the Re reaches 13000, at which point efficiency begins to decline. At w_g/e =1, SAH-DMAR has a maximum effective efficiency of 77.6%, against 70.4% for traditional SAH. Thus, Re > 13000 is not recommended since the higher frictional losses outweigh the heat transfer enhancement.

Fig. 10a depicts the variation of T_p with Re for various rib pitch (p/e) values when the e/D of 0.045, the w_g/e of 1, the N_g of 3, and the α of 45°. The T_p drops as Re increases for all p/e values examined. The reason for this is that when Re rises, the turbulence intensity rises, implying that the air absorbs more heat from the absorber plate. For any Re, when the p/e increases, the T_p drops, reaches a minimum, and then rises. At a p/e of 12, T_p reaches its minimal value. The flow inter-rib reattachment and boundary layer regeneration are the causes of this fluctuation. The presence of ribs in the flow channel causes turbulence, which could improve heat transfer in terms of Q_u, as illustrated in Fig. 10b. Q_u has reached the highest value at p/e = 12 and corresponds to a higher Re in the investigated range of p/e. The number of re-attachment points produced by rib-roughness changes drastically as p/e changes. Even though the numbers of roughness components attached to the absorber plate are higher and they are closer together in p/e <12, there is little production of re-attachment points between the two following ribs, leading to a low Qu. The number of reattachment points is maximum when p/e = 12 is compared to other p/e values, such as 16.

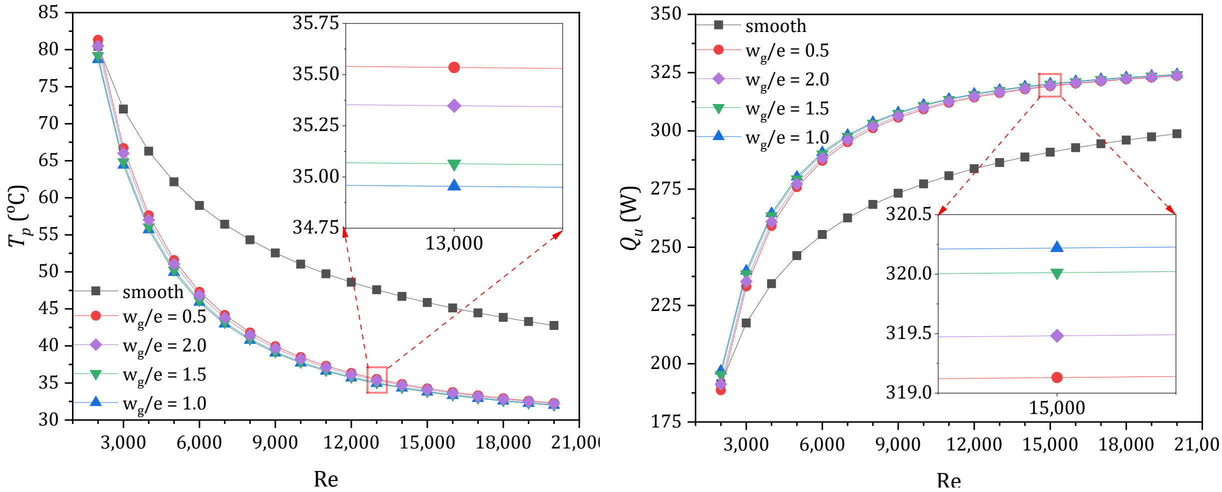

(a) (b)

Figure 8. The influence of w_g/e on (a) absorber plate temperature, and (b) useful energy gain.

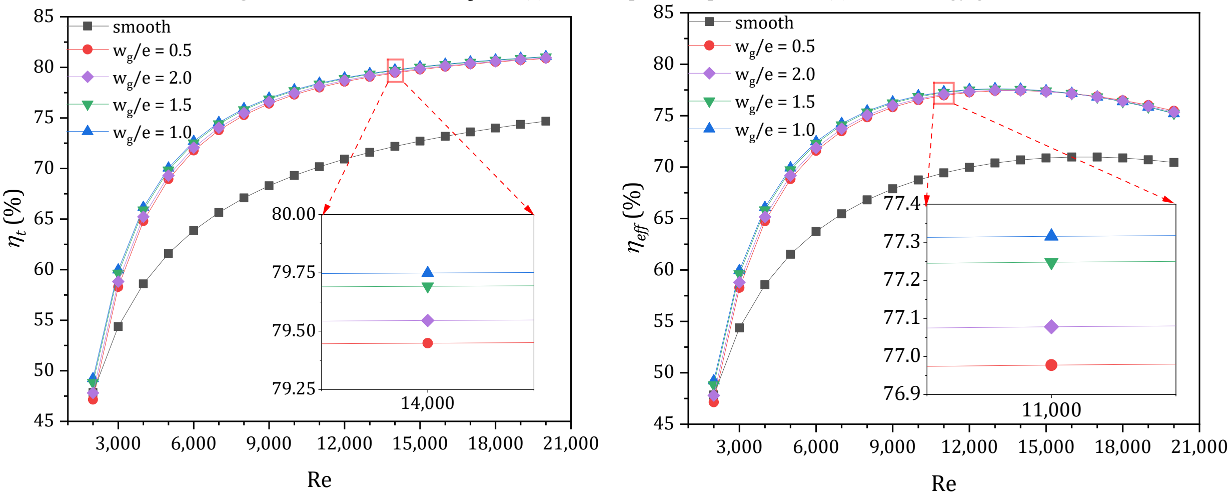

(a) (b)

Figure 9. The impact of w_g/e on (a)thermal efficiency, and (b)effective efficiency.

Fig. 11a depicts the thermal efficiency of a SAH with and without DMAR as a function of Re. When compared to smooth SAH, it is obvious that the thermal efficiency is considerably improved for all p/e values. Thermal efficiency improves as the pitch ratio is increased until p/e = 12, but for other pitch ratios, the opposite occurs. The maximum thermal efficiencies of SAH-DMAR and smooth SAH are 81.1 % and 74.7 %, respectively. Over a range of Re, Fig. 11b demonstrates the variation in the effective efficiency of a SAH with and without DMAR. The effective efficiency is clearly boosted over smooth SAH for all p/e values until Re exceeds 13000, after which it starts to fall due to the substantial extra pressure drop compared to low thermal enhancement. As a result, it is not recommended to use DMAR with SAH at Re > 13000. It is found that the effective efficiency of SAH-DMAR increased by 9.3% more than that for smooth duct when Re =13000. Based on the preceding findings, the highest effective efficiency is found at a p/e of 16.

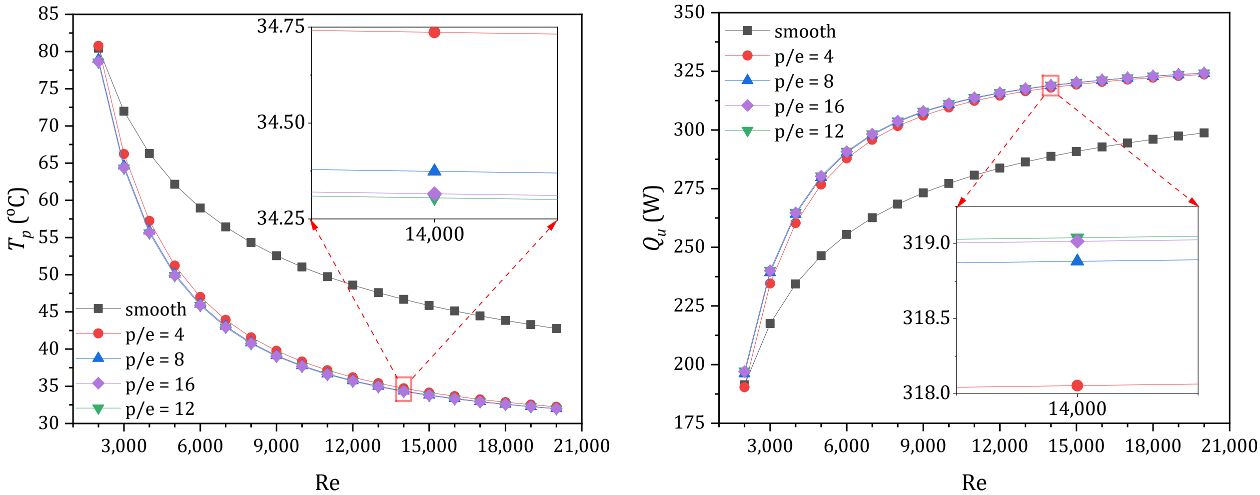

(a) (b)

Figure 10. The influence of p/e on (a) absorber plate temperature, and (b) useful energy gain.

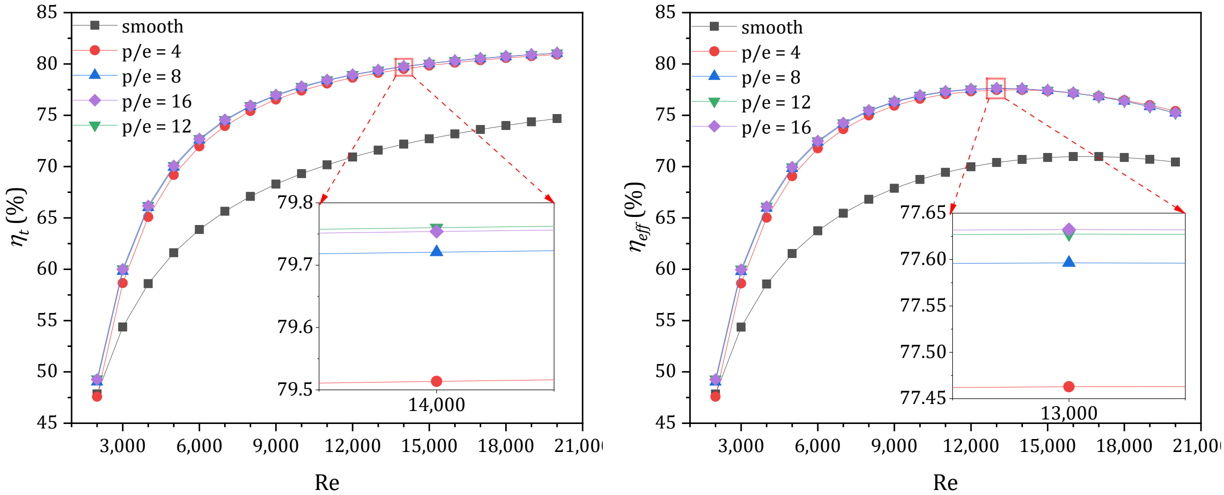

(a) (b)

Figure 11. The influence of *p/e* on (a)thermal efficiency, and (b)effective efficiency.

The influence of the angle of attack(α) is explored on T_p and Q_u of a solar air collector as illustrated in Fig. 12, where p/e, Ng, w_g/e, and e/D are at constant values of 16, 3, 1, and 0.045, respectively. The variations of T_p against the Re are seen in Fig. 12a. It may be seen that a roughness duct with DMAR transmits more useful energy gain to the airstream than that smooth duct, i.e., lower T_p for roughened SAH. It is discovered that the values of $T_p$are dropping with rises of Re in all cases. Consequently, the value of Q_u is raised with the growth of Re as depicted in Fig. 12b. Also, Q_u values are discovered to be enhanced with the subsequent rise in α. It occurs due to the shift in the path followed by the secondary flow across the absorber plate. Usually, the secondary flow occurred owing to the breakdown of viscous sub-layers flows or led by the rib element across the absorber plate, and it is transported along with the arc-shape rib element. Thus, the downstream eddies along DMAR which come in connection with the main airflow are transmitted to the heated surface which enhances the heat transfer rate.

The variation of thermal efficiency as a function of Re is shown in Fig. 13a for α values ranging from 30° to 75°. The greatest value of thermal efficiency is clearly discovered at 75°, while the lowest value is found at 30°. The behavior of thermal efficiency patterns may be explained by the fact that DMAR numbers become greatest in contact with the main airstream at α =75°, compared to the other values. In other words, at the heated surface, a significant recirculation flow zone occurs, allowing air to absorb more heat than a smooth duct. Fig. 13b depicts the effect of α on effective efficiency. Roughness ducts with DMAR have a higher effective efficiency than smooth ducts, as can be seen. For all values of Re, it is discovered that the values of effective efficiency rise as the value of α grows. The intense re-circulation flow zone that occurs at the heated surface causes powerful eddies that disrupt the axial airstream, and the pumping power required to move air across the duct increases due to the significant pressure drop. At Re = 13000, the highest increase in effective efficiency for SAH-DMAR is 9.4% higher than for smooth SAH.

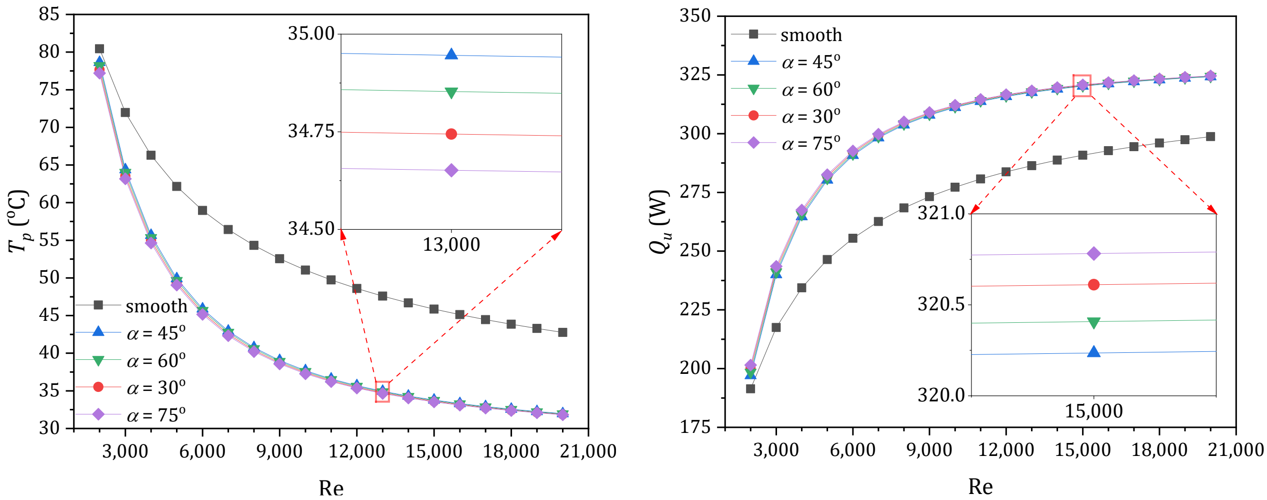

(a) (b)

Figure 12. Effect of α on (a) absorber plate temperature, and (b) useful energy gain.

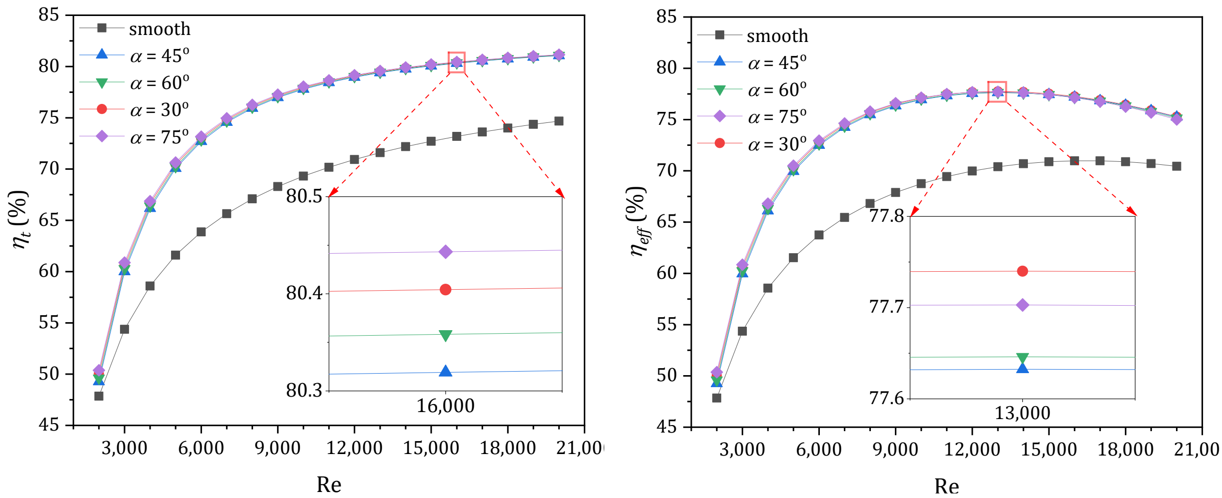

(a) (b)

Figure 13. The impact of α on (a)thermal efficiency, and (b)effective efficiency.

Table 2. Weather data for Baghdad on 3/1/2022

Time	8:00	9:00	10:00	11:00	12:00	13:00	14:00	15:00	16:00
I (W/m^2)	244.2	546.8	759.1	891.3	940.9	908.1	792.3	596.8	316.2
T_{am} (°C)	7.1	9.2	9.9	11.2	11.3	12.0	12.1	12.0	11.9

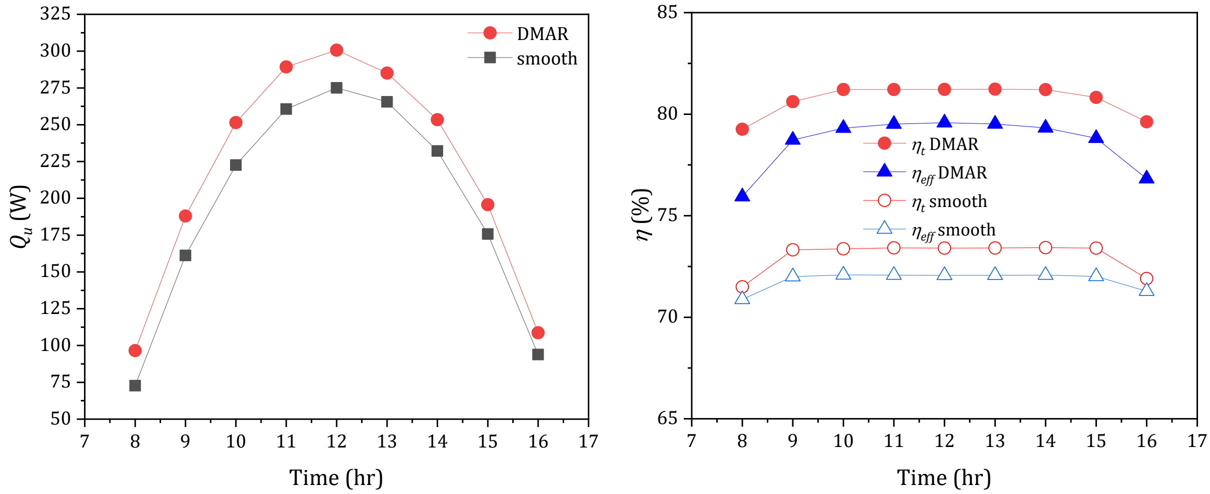

(a) (b)

Figure 14. Effect of optimum DMAR parameters on (a) useful energy gain, and (b) the thermal and effective efficiencies under real weather conditions on 3/1/2022.

Thermal efficiency enhancement criteria (*TEEC*) is a factor used to measure the augmentation in thermal efficiency of a SAH having an absorbing plate roughened by an artificial rib, which is calculated as

$$TEEC = \frac{\eta_{t,r}-\eta_{t,s}}{\eta_{t,s}} \quad (25)$$

where, $\eta_{t,r}$, and $\eta_{t,s}$ are the thermal efficiency of roughened and smooth SAH, respectively.

The results of this study are compared to those of previously published investigations of different roughness geometries under similar conditions using Eq. 25. Fig. 15 depicts the variation of *TEEC* as a function of Re. According to the behavior of the curves, it can be reported that the validation results are in good agreement.

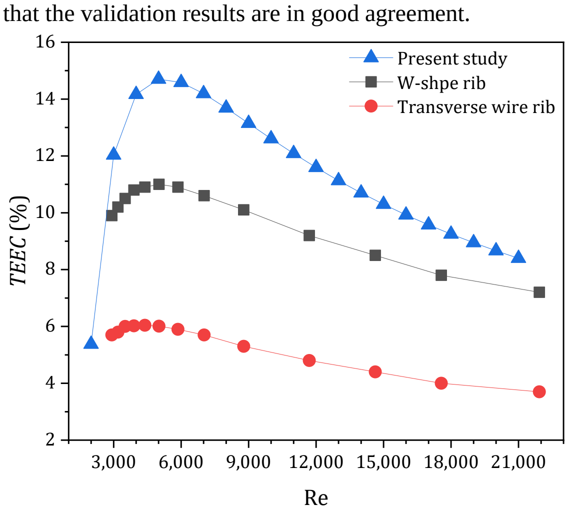

Figure 15. *TEEC* vs Re for comparison between the present study with W-shape rib [31] and transverse wire rib[32].

Performance evaluation criteria (*PEC*) is used to measure the enhancement in heat transfer rate against the penalty in pressure drop across the SAH as follows

$$PEC = \frac{\left(\frac{Nu_r}{Nu_s}\right)^3}{\frac{f_r}{f_s}} \quad (26)$$

where Nu_r, Nu_s, and fr, fs are Nusselt number and friction factor for roughened and smooth SAH, respectively.

The *PEC* obtained in this study is compared to previous research that used various rib shapes to enhance the performance of a SAH. Table 3 shows the comparison of the current work to previous ones, and as can be seen, the current method is satisfactory.

Table 3. Comparison to previously published studies

Rib shape	*PEC*
Arc shape [16]	2.78
Multiple V-shape [33]	3.51
Multi V-shape with gaps [34]	3.64
Multi-arc shape [35]	2.24
Multigap V-down ribs with staggered ribs [36]	2.23
S-shape [12]	3.34
Present study	3.51

4. Conclusions

In this study, the operating parameters of SAH with DMAR roughness on the absorbing plate were studied. The SAH's performance is assessed using a top-down iterative technique in MATLAB. The purpose of this study was to identify the optimum roughness parameters for maximum effective efficiency. The main conclusions of our investigation can be stated as follows:

1. The effective efficiency for SAH-DMAR was 9.4% higher than for smooth SAH. Optimum effective efficiency occurred atp/e, e/D, w_g/e, N_g, and α for DMARof 16, 0.045, 1, 3, and 75, respectively.
2. SAH-DMAR and smooth SAH have a maximum thermal efficiency of 81.1 % and 74.7 %, respectively.
3. The maximal heat gain for a SAH-DMAR is 324.2 W, against 298.7 W for a smooth duct.

4. Thermal and effective efficiencies of the SAH-DMAR are found to be 9.5 % and 8.6% higher than those of smooth duct, respectively when implemented in real weather conditions.

References

[1] A. Al aboushi, Solar Thermal Hybrid Heating System, Jordan Journal of Mechanical and Industrial Engineering. 11 (2017) 181–184.

[2] R. Al-Rbaihat, A. Sakhrieh, J. Al-Asfar, A. Alahmer, O. Ayadi, A. Al-Salaymeh, Z. Al-Hamamre, A. Al-Bawwab, M. Hamdan, Performance assessment and theoretical simulation of adsorption refrigeration system driven by flat plate solar collector, Jordan Journal of Mechanical and Industrial Engineering. 11 (2017) 1–11.

[3] K. Nidhul, A.K. Yadav, S. Anish, S. Kumar, Critical review of ribbed solar air heater and performance evaluation of various V-rib configuration, Renew. Sustain. Energy Rev. 142 (2021) 110871. https://doi.org/10.1016/j.rser.2021.110871.

[4] A.A. Farhan, H.A. Sahi, Energy Analysis of Solar Collector With perforated Absorber Plate, J. Eng. 23 (2017) 89–102.

[5] D.J. Hasan, A.A. Farhan, The Effect of Staggered porous fins on the performance of Photovoltaic panel in Baghdad, J. Eng. 26 (2020) 1–13. https://doi.org/10.31026/j.eng.2020.08.01.

[6] M. Al-Damook, Z.A.H. Obaid, M. Al Qubeissi, D. Dixon-Hardy, J. Cottom, P.J. Heggs, CFD modeling and performance evaluation of multipass solar air heaters, Numer. Heat Transf. Part A Appl. 76 (2019) 438–464. https://doi.org/10.1080/10407782.2019.1637228.

[7] S.Y. Taha, A.A. Farhan, Performance augmentation of a solar air heater using herringbone metal foam fins: An experimental work, Int. J. Energy Res. 45 (2021) 2321–2333. https://doi.org/10.1002/er.5927.

[8] S. Das, Simulation of optimal exergy efficiency of solar flat plate collector, Jordan Journal of Mechanical and Industrial Engineering. 10 (2016) 51–65.

[9] N. Minh Phu, N. Thanh Luan, A Review of Energy and Exergy Analyses of a Roughened Solar Air Heater, J. Adv. Res. Fluid Mech. Therm. Sci. 77 (2020) 160–175. https://doi.org/10.37934/arfmts.77.2.160175.

[10] S. Singh, S. Chander, J.S. Saini, Thermo-hydraulic performance due to relative roughness pitch in V-down rib with gap in solar air heater duct—Comparison with similar rib roughness geometries, Renew. Sustain. Energy Rev. 43 (2015) 1159–1166. https://doi.org/10.1016/j.rser.2014.11.087.

[11] H.K. Ghritlahre, An experimental study of solar air heater using arc shaped wire rib roughness based on energy and exergy analysis, Arch. Thermodyn. 42 (2021) 115–139. https://doi.org/10.24425/ather.2021.138112.

[12] K. Kumar, D.R. Prajapati, S. Samir, Heat transfer and friction factor correlations development for solar air heater duct artificially roughened with ‘S’ shape ribs, Exp. Therm. Fluid Sci. 82 (2017) 249–261. https://doi.org/10.1016/j.expthermflusci.2016.11.012.

[13] A.A. Farhan, H.E. Ahmed, M.A. Mussa, Thermal–Hydraulic Performance of a V-Groove Solar Air Collector with Transverse Wedge-Shaped Ribs, Arab. J. Sci. Eng. (2022). https://doi.org/10.1007/s13369-021-06442-5.

[14] S.S. Bhuvad, R. Azad, A. Lanjewar, Thermal performance analysis of apex-up discrete arc ribs solar air heater-an experimental study, Renew. Energy. 185 (2022) 403–415. https://doi.org/10.1016/j.renene.2021.12.037.

[15] N.K. Pandey, V.K. Bajpai, A. Sharma, S. Yadav, CFD and thermo-hydraulic analysis of multiple arc roughened absorber plate with gaps used in solar air heaters, Int. J. Ambient Energy. 0 (2020) 1–7. https://doi.org/10.1080/01430750.2020.1824941.

[16] S.K. Saini, R.P. Saini, Development of correlations for Nusselt number and friction factor for solar air heater with roughened duct having arc-shaped wire as artificial roughness, Sol. Energy. 82 (2008) 1118–1130. https://doi.org/10.1016/j.solener.2008.05.010.

[17] H.K. Ghritlahre, P.K. Sahu, S. Chand, Thermal performance and heat transfer analysis of arc shaped roughened solar air heater – An experimental study, Sol. Energy. 199 (2020) 173–182. https://doi.org/10.1016/j.solener.2020.01.068.

[18] A.P. Singh, Varun, Siddhartha, Heat transfer and friction factor correlations for multiple arc shape roughness elements on the absorber plate used in solar air heaters, Exp. Therm. Fluid Sci. 54 (2014) 117–126. https://doi.org/10.1016/j.expthermflusci.2014.02.004.

[19] N.K. Pandey, V.K. Bajpai, Thermo-hydraulic performance enhancement of solar air heater (SAH) having multiple arcs with gap shaped roughness element on absorber plate, Int. J. Eng. Sci. Technol. 8 (2016) 34–42. https://doi.org/10.4314/ijest.v8i1.3.

[20] Y. Agrawal, J.L. Bhagoria, V.S. Pagey, Enhancement of thermal efficiency of solar air collector by using discrete double arc reverse shaped roughness on the absorber plate, Mater. Today Proc. (2021). https://doi.org/10.1016/j.matpr.2021.10.362.

[21] R. Kumar, V. Goel, S. Bhattacharyya, V. V. Tyagi, A.M. Abusorrah, Experimental investigation for heat and flow characteristics of solar air heater having symmetrical gaps in multiple-arc rib pattern as roughness elements, Exp. Heat Transf. 00 (2021) 1–18. https://doi.org/10.1080/08916152.2021.1905752.

[22] R. Azad, S. Bhuvad, A. Lanjewar, Study of solar air heater with discrete arc ribs geometry: Experimental and numerical approach, Int. J. Therm. Sci. 167 (2021) 107013. https://doi.org/10.1016/j.ijthermalsci.2021.107013.

[23] M.A. Alfellag, H.E. Ahmed, M.G. Jehad, A.A. Farhan, The hydrothermal performance enhancement techniques of corrugated channels: a review, J. Therm. Anal. Calorim. (2022). https://doi.org/10.1007/s10973-022-11247-1.

[24] M.K. Sahu, R.K. Prasad, Thermohydraulic performance analysis of an arc shape wire roughened solar air heater, Renew. Energy. 108 (2017) 598–614. https://doi.org/10.1016/j.renene.2017.02.075.

[25] A. Cortés, R. Piacentini, Improvement of the efficiency of a bare solar collector by means of turbulence promoters, Appl. Energy. 36 (1990) 253–261. https://doi.org/10.1016/0306-2619(90)90001-T.

[26] J.A. Duffie, W.A. Beckman, N. Blair, Solar Engineering of Thermal Processes, Photovoltaics and Wind, fifth edit, JohnWiley& Sons, Inc., Hoboken,New Jersey, 2020.

[27] K.S. Ong, Thermal performance of solar air heaters: Mathematical model and solution procedure, Sol. Energy. 55 (1995) 93–109. https://doi.org/10.1016/0038-092X(95) 000 21 -I.

[28] K.G.T. Hollands, E.C. Shewen, Optimization of flow passage geometry for air-heating, plate-type solar collectors, J. Sol. Energy Eng. Trans. ASME. 103 (1981) 323–330. https://doi.org/10.1115/1.3266260.

[29] M. Hedayatizadeh, Y. Ajabshirchi, F. Sarhaddi, S. Farahat, A. Safavinejad, H. Chaji, Analysis of exergy and parametric study of a v-corrugated solar air heater, Heat Mass Transf. 48 (2012) 1089–1101. https://doi.org/10.1007/s00231-011-0957-7.

[30] R. Kumar, P. Chand, Performance prediction of extended surface absorber solar air collector with twisted tape inserts, Sol. Energy. 169 (2018) 40–48. https://doi.org/10.1016/j.solener.2018.04.021.

[31] A. Lanjewar, J.L. Bhagoria, R.M. Sarviya, Heat transfer and friction in solar air heater duct with W-shaped rib roughness

on absorber plate, Energy. 36 (2011) 4531–4541. https://doi.org/10.1016/j.energy.2011.03.054.

[32] S.K. Verma, B.N. Prasad, Investigation for the optimal thermohydraulic performance of artificially roughened solar air heaters, Renew. Energy. 20 (2000) 19–36. https://doi.org/10.1016/S0960-1481(99)00081-6.

[33] V.S. Hans, R.P. Saini, J.S. Saini, Heat transfer and friction factor correlations for a solar air heater duct roughened artificially with multiple v-ribs, Sol. Energy. 84 (2010) 898–911. https://doi.org/10.1016/j.solener.2010.02.004.

[34] A. Kumar, R.P. Saini, J.S. Saini, Development of correlations for Nusselt number and friction factor for solar air heater with roughened duct having multi v-shaped with gap rib as artificial roughness, Renew. Energy. 58 (2013) 151–163. https://doi.org/10.1016/j.renene.2013.03.013.

[35] A.P. Singh, Varun, Siddhartha, Effect of artificial roughness on heat transfer and friction characteristics having multiple arc shaped roughness element on the absorber plate, Sol. Energy. 105 (2014) 479–493. https://doi.org/10.1016/j.solener.2014.04.007.

[36] N.S. Deo, S. Chander, J.S. Saini, Performance analysis of solar air heater duct roughened with multigap V-down ribs combined with staggered ribs, Renew. Energy. 91 (2016) 484–500. https://doi.org/10.1016/j.renene.2016.01.067.